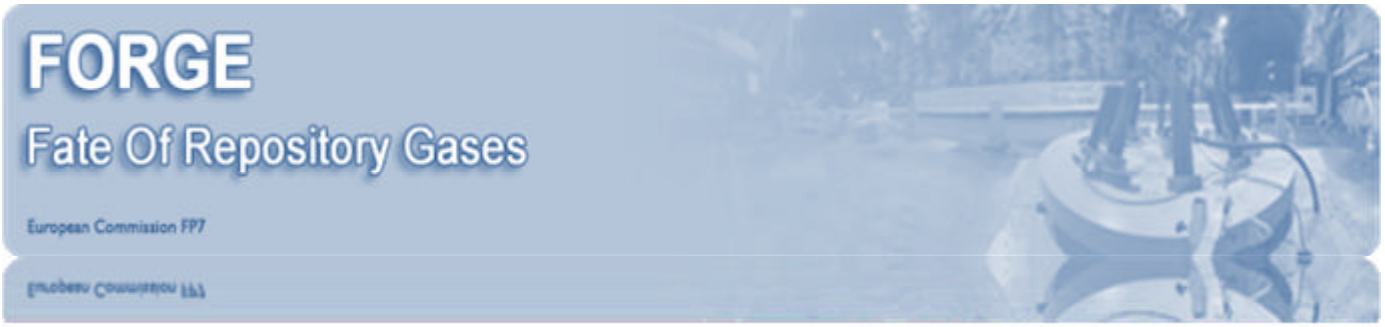

Opalinus clay gas induced fracturing

Technical Report CIEMAT/DMA/2G207/5/12

FORGE Report D5.11 – VER.0

	Name	Organisation	Signature	Date
Compiled	M.V. Villar	CIEMAT		27th November 2012
Verified	RP Shaw	BGS		13th January 2013
Approved	RP Shaw	BGS		13th January 2013

Keywords:

Opalinus clay, water retention capacity, air entry pressure, suction control, gas permeability

Bibliographical reference

M.V. Villar, F.J. Romero, P.L. Martín. 2012. Opalinus clay gas induced fracturing. FORGE Report D5.11. 24pp.

Euratom 7th Framework Programme Project: FORGE

Fate of repository gases (FORGE)

The multiple barrier concept is the cornerstone of all proposed schemes for underground disposal of radioactive wastes. The concept invokes a series of barriers, both engineered and natural, between the waste and the surface. Achieving this concept is the primary objective of all disposal programmes, from site appraisal and characterisation to repository design and construction. However, the performance of the repository as a whole (waste, buffer, engineering disturbed zone, host rock), and in particular its gas transport properties, are still poorly understood. Issues still to be adequately examined that relate to understanding basic processes include: dilational versus visco-capillary flow mechanisms; long-term integrity of seals, in particular gas flow along contacts; role of the EDZ as a conduit for preferential flow; laboratory to field up-scaling. Understanding gas generation and migration is thus vital in the quantitative assessment of repositories and is the focus of the research in this integrated, multi-disciplinary project. The FORGE project is a pan-European project with links to international radioactive waste management organisations, regulators and academia, specifically designed to tackle the key research issues associated with the generation and movement of repository gasses. Of particular importance are the long-term performance of bentonite buffers, plastic clays, indurated mudrocks and crystalline formations. Further experimental data are required to reduce uncertainty relating to the quantitative treatment of gas in performance assessment. FORGE will address these issues through a series of laboratory and field-scale experiments, including the development of new methods for up-scaling allowing the optimisation of concepts through detailed scenario analysis. The FORGE partners are committed to training and CPD through a broad portfolio of training opportunities and initiatives which form a significant part of the project.

Further details on the FORGE project and its outcomes can be accessed at www.FORGEproject.org.

Contact details:

María Victoria Villar
CIEMAT
Tel: +34 913466139 Fax +34 913466542
email: mv.villar@ciemat.es
web address: http://www.ciemat.es/portal.do
Address: Avd. Complutense 40, 28040 Madrid

Francisco Javier Romero
CIEMAT
Tel: +34 913466308 Fax +34 913466542
email: francisco.romero@ciemat.es
web address: http://www.ciemat.es/portal.do
Address: Avd. Complutense 40, 28040 Madrid

Pedro Luis Martín
CIEMAT
Tel: +34 913466142 Fax +34 913466542
email: pedro.lmartin@ciemat.es
web address: http://www.ciemat.es/portal.do
Address: Avd. Complutense 40, 28040 Madrid

Foreword

This report refers to the work carried out by CIEMAT in FORGE WP5.1 "Gas transport laboratory experiments", which included the determination of breakthrough pressures in Opalinus clay. For that, an experimental setup able to measure the gas permeability and breakthrough pressure was developed. A summary of the results obtained is reported.

Acknowledgements

The research leading to these results has received funding from the European Atomic Energy Community's Seventh Framework Programme (FP7/2007-2011) under Grant Agreement n°230357, the FORGE project. Part of the laboratory work was performed by Ramón Campos and Juan Aroz, from CIEMAT.

Contents

Foreword **1**

Acknowledgements **1**

Contents **1**

Summary **3**

1 Introduction **3**

2 Material **3**

3 Methodology **4**

3.1 Equipment 4

3.2 Sample preparation and test procedure 8

3.3 Gas permeability computation 9

4 Results **10**

Conclusions **21**

References **22**

FIGURES

Figure 1: Experimental setup with piston controller (low pressure line) 5

Figure 2: Experimental setup with bladder accumulator (high pressure line) 5

Figure 3: Schematic design of the triaxial cell type 1 used for the gas permeability and breakthrough tests 6

Figure 4: Triaxial cell type 2 7

Figure 5: Gas-booster and high-pressure buffer to supply gas to the injection pressure deposit and to the pressure accumulator applying confining pressure in the high-pressure line.. 7

Figure 6: Pressure accumulator to apply high confining pressure 7

Figure 7: Appearance of an Opalinus clay sample drilled for a gas test, wrapped in the shrinking rubber sleeve (black) and in the latex membrane (red) 8

Figure 8: Pressure paths followed in the gas breakthrough tests (tests OPA2 and OPA5 followed only Phase 1 under confining pressure 8 MPa)..... 9

Figure 9: Setup for the water permeability tests..... 9

Figure 10: Evolution of injection and confining pressure and outflow in test OPA1..... 11

Figure 11: Change of gas permeability with the increase of confining pressure for an injection pressure of 7 MPa and atmospheric backpressure in test OPA1..... 12

Figure 12: Gas permeability measured for different confining and effective pressures in test OPA1 12

Figure 13: Final appearance of sample OPA1 13

Figure 14: Final appearance of OPA1 under the stereomicroscope 13

Figure 15: Evolution of injection and confining pressure and outflow in test OPA2..... 14

Figure 16: Change of gas permeability with the increase of injection pressure for a confining pressure of 8 MPa and atmospheric backpressure in test OPA2..... 14

Figure 17: Initial and final appearance of sample OPA2..... 15

Figure 18: Appearance of specimen OPA3 after drilling from the core 15

Figure 19: Evolution of injection and confining pressure and outflow in test OPA3..... 16

Figure 20: Change of gas permeability with the increase of injection pressure for different confining pressures and atmospheric backpressure in test OPA3..... 16

Figure 21: Evolution of injection and confining pressure and outflow in test OPA4..... 17

Figure 22: Change of gas permeability with the increase of injection pressure for different confining pressures and atmospheric backpressure in test OPA4..... 18

Figure 23: Evolution of injection and confining pressure and outflow in test OPA5..... 19

Figure 24: Change of gas permeability with the increase of injection pressure for confining pressure 8 MPa and atmospheric backpressure in test OPA5..... 19

Figure 25: Final appearance of specimen OPA5 20

Figure 26: Gas permeability values obtained in samples of Opalinus clay (tentative values, especially those below 10^{-22} m^2; flow along the sample periphery could have taken place in test OPA1)..... 21

TABLES

Table I: Characteristics of the specimens used for gas permeability tests.....10

Summary

An experimental setup was designed to measure gas permeability and gas breakthrough pressures in highly confined Opalinus clay samples. It was able to apply gas injection pressures of up to 18 MPa to cylindrical samples submitted to higher confining pressures while measuring the gas otflow. These tests, performed in samples drilled from core BDR-1 perpendicularly to the bedding plane, showed that the breakthrough pressure of samples of degree of saturation 84±15% was higher than 18 MPa. The air entry value calculated from the mercury intrusion porosimetry tests was 28 MPa. The gas permeability was below $1{\cdot}10^{-15}$ m/s.

1 Introduction

This report includes the work carried out by CIEMAT in FORGE WP5.1 "Gas transport laboratory experiments", which included two kinds of tests in indurated clay (the Opalinus clay), the determination of 2-phase flow parameters (Villar & Romero 2012) and gas permeability and gas breakthrough pressure determinations, which are the topic of this report.

For the determination of the gas permeability and gas breakthrough pressure a setup was designed and fine-tuned. It allowed the application of gas injection pressures of up to 18 MPa to cylindrical samples while keeping higher confining pressures and measuring the gas outflow. The measurements of the stress state at Mont Terri indicate that s_1 is 6-7 MPa (Corkum & Martin 2007), what means that the confining pressures applied in the laboratory tests have been higher than this value.

2 Material

The material used in the tests came from a borehole drilled in the Opalinus Clay Mesozoic formation in the Mont Terri Underground Research Laboratory in the Folded Jura mountains (http://www.mont-terri.ch). This formation is a mainly marly claystone with differing proportions of sand and carbonates around 180 million years old (Aalenian). At the URL, the Opalinus Clay has a layer thickness of around 140 m.

From a mineralogical point of view the Opalinus Clay consists of 40-80% clay minerals (including mixed layers of swelling illite and smectite), 10-40% quartz, 5-40% calcite and smaller proportions of siderite, pyrite and organic carbon. The dry density range is between 2.20 and 2.41 g/cm^3, the water content between 5.0 and 8.9% and the hydraulic conductivity between $2{\cdot}10^{-14}$ and $1{\cdot}10^{-12}$ m/s.

Of the three facies of Opalinus Clay that can be distinguished, the materials used in this investigation belong to the shaly one, which is a homogeneous, barely visible laminated claystone with low sand content. For the gas permeability and breakthrough pressure tests a core from borehole BDR-1 was used. The total suction of this core was measured at laboratory temperature (21°C) with two capacitive sensors inserted in a suitable perforated hole. The equilibrium value was found to be 31.3±0.1 MPa for a dry density of 2.33 g/cm^3 and water content of 6.4% (determined in samples drilled from the core). The measured grain density for this sample was 2.71 g/cm^3.

Additionally, a sample from the BHG-D1 core used for the determination of the water retention curves (Villar & Romero 2012) was lyophilised and analysed by mercury intrusion porosimetry.

The dry density was 2.4 g/cm^3 and the water content 3.4% (slightly air-dried). Most of the pore sizes were comprised in the range 2-50 nm, *i.e.* in the mesopore range, with a dominant pore mode of 11 nm. The air entry value corresponding to this dominant pore mode calculated from the Laplace's equation is 27.8 MPa.

3 Methodology

3.1 EQUIPMENT

A setup was designed to perform steady gas permeability measurements under different gas pressures. The cylindrical sample was confined in a stainless steel triaxial cell that was pressurised to the desired confining pressure. The injection pressure could be independently varied and kept constant during the period of time necessary to get steady flow, while the backpressure was kept atmospheric and the outflow measured.

Two different lines were used to apply the confining pressure: a low-pressure line (Figure 1), in which the confining pressure was applied with a GDS pressure/volume piston controller with a working capacity up to 16 MPa; and a high-pressure line to apply confining pressures up to 33 MPa (Figure 2). In the latter, the water in the cell was pressurised using the gas in a pressure bladder accumulator, which took the gas from a high-pressure deposit in which nitrogen was previously compressed by a gas-booster. The gas-booster took the nitrogen from a gas cylinder and the high-pressure deposit was equipped with a high-performance high-pressure unit (valve and controller) that controlled the actual pressure value applied to the accumulator. This high-pressure deposit supplied also the nitrogen gas to a 300-cm^3 pressurised deposit equipped with a pressure transmitter from which nitrogen was injected on top of the sample. Injection pressures of up to 18 MPa could be applied. The outlet of the cell connected to the bottom of the sample was open to atmosphere, with a series of different range gas mass flowmeters measuring the gas outflow. Outflow gas rates, up and downstream pressure, confining pressure and temperature were monitored online.

A more detailed description of the components of the experimental setup includes:

- *Test cells*. They were made of stainless steel, able of withstanding pressures up to 21 MPa (Figure 3, Figure 4). Each cell had three inlets drilled: one for sample top drainage, one for sample bottom drainage, and another one for confining pressure. Three no volume change valves were connected to the ports. The tests were not performed under real triaxial conditions though.
- *Gas booster*. To obtain the high gas pressures needed for the confining and injection pressures, nitrogen taken from a gas cylinder was compressed by a POWER-STAR gas-booster (up to 35 MPa, dual stage, air-operated) in a high-pressure (34.5 MPa) cylinder (Figure 5). The final pressure applied to the system was controlled by a high-performance high-pressure unit (valve and controller).
- *Gas buffer*. The gas was injected on top of the samples from a WHITEY gas sampling cylinder (DOT-3E 1800, SS-316, 300 cm^3) acting as a gas buffer to prevent fluctuations in the injection pressure. It also allowed to keep constant the expected flow even in case of pneumatic fracturing. The deposit was pressurised with the setup described above and was equipped with a pressure transmitter. Injection pressures of up to 18 MPa could be applied.

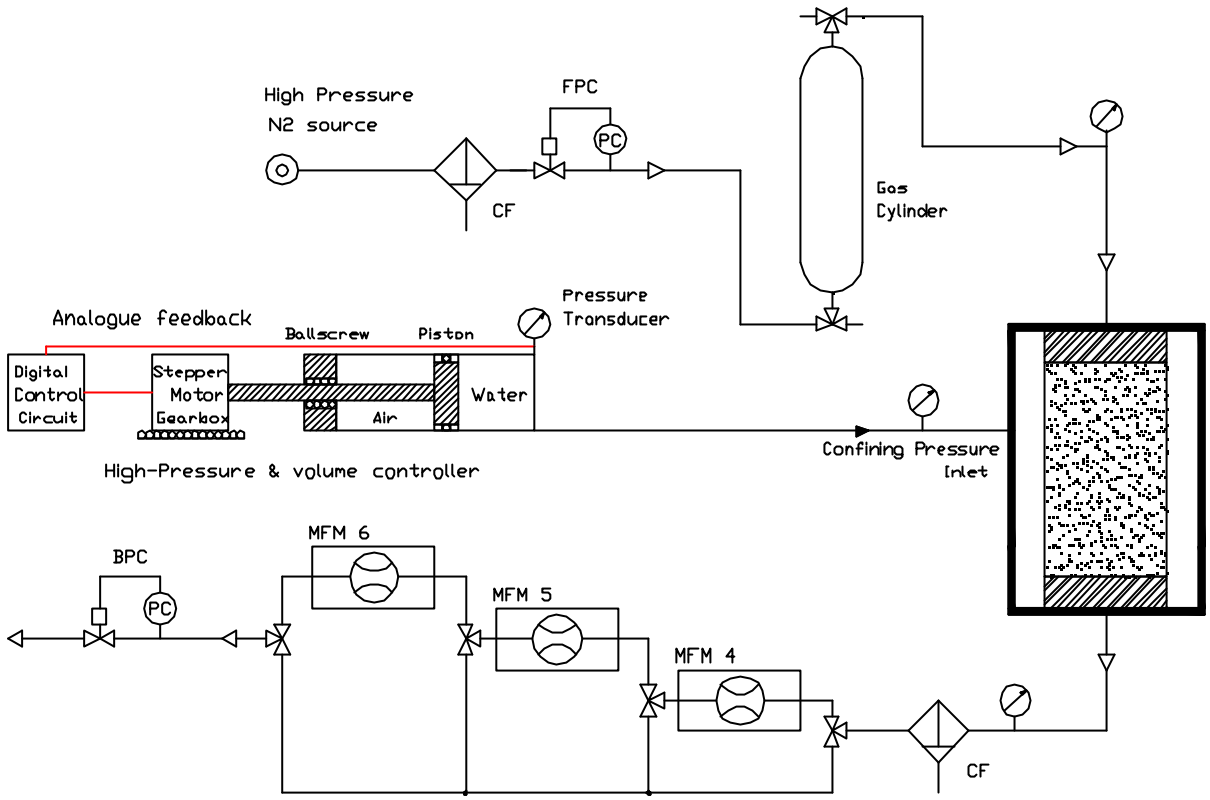

Figure 1: Experimental setup with piston controller (low pressure line)

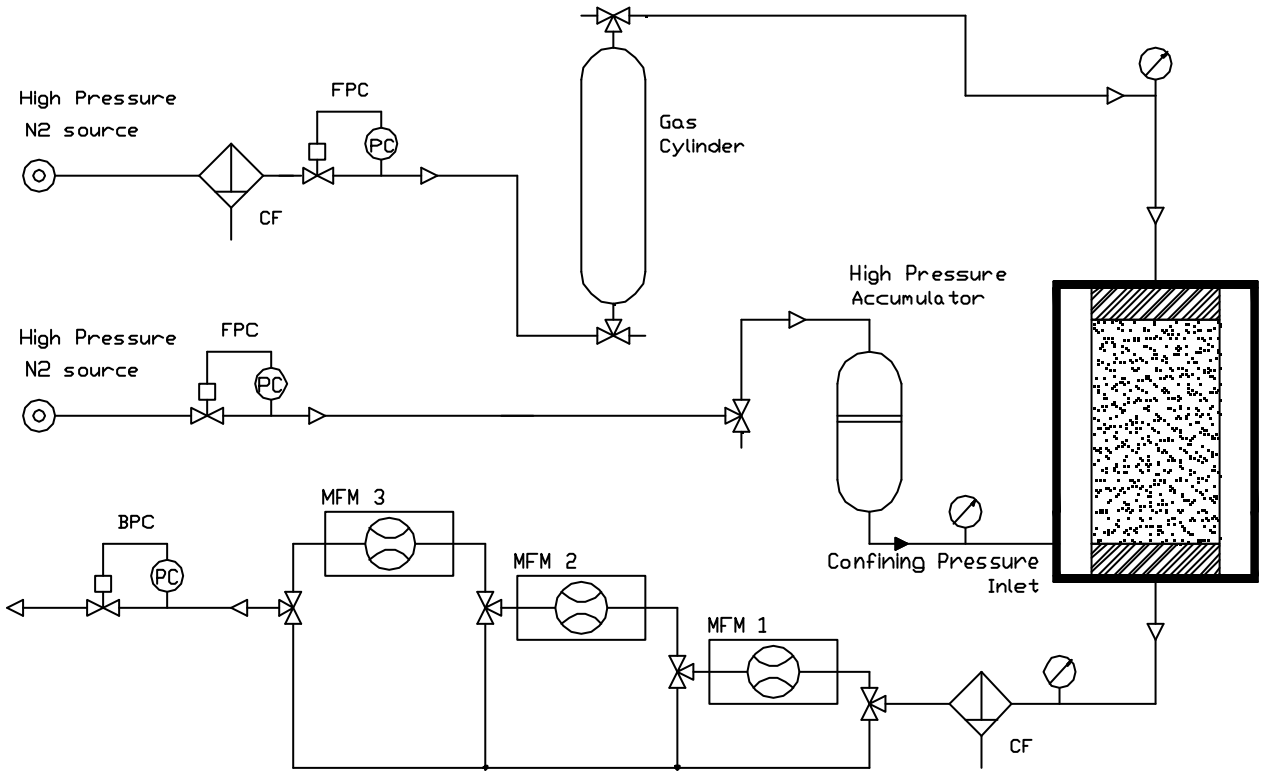

Figure 2: Experimental setup with bladder accumulator (high pressure line)

- *Water/nitrogen separator*. An OLAER's pressure bladder accumulator (up to 33 MPa) was used to apply the high confining pressures (Figure 6). The internal elastic membrane kept apart the nitrogen and the water phases of the high-pressure confining pressure system.

- *Gas mass flowmeters*. The outflow gas rates, coming out from the bottom of the sample to the atmosphere, were measured using a series of three gas mass flowmeters with different ranges: 1000, 100 and 10 STP cm^3/min (the latter was 2 STP cm^3/min in the high-pressure line), with a turndown of 1:50 (minimum value measured with acceptable accuracy 2% FS). HI-TEC flowmeters operate on a principle of heat transfer by sensing the temperature increment along a heated section of a capillary tube. They were calibrated to the consigned conditions: nitrogen gas, pressure 70 bar a, and temperature 20°C. The output signal was 0-5 VDC.
- *Pressure transmitters*. DRUCK pressure transmitters, PTX1400 series, were placed at several points: the inlet port of the triaxial cell (injection pressure), the outlet port of the water/nitrogen separator (confining pressure), and the outlet of the system (atmospheric pressure). The transmitters range was 100 bar a (0.25% BSL). The output signal was 4-20 mA.
- *Tubing, fitting and valves*. All the SWAGELOK fitting materials and valves were made of stainless steel, SS316. The SANVICK tubing material was SS316 1/8". The maximum leakage rate according to manufacturer was around 0.1 cm^3/min at 68 bar g.

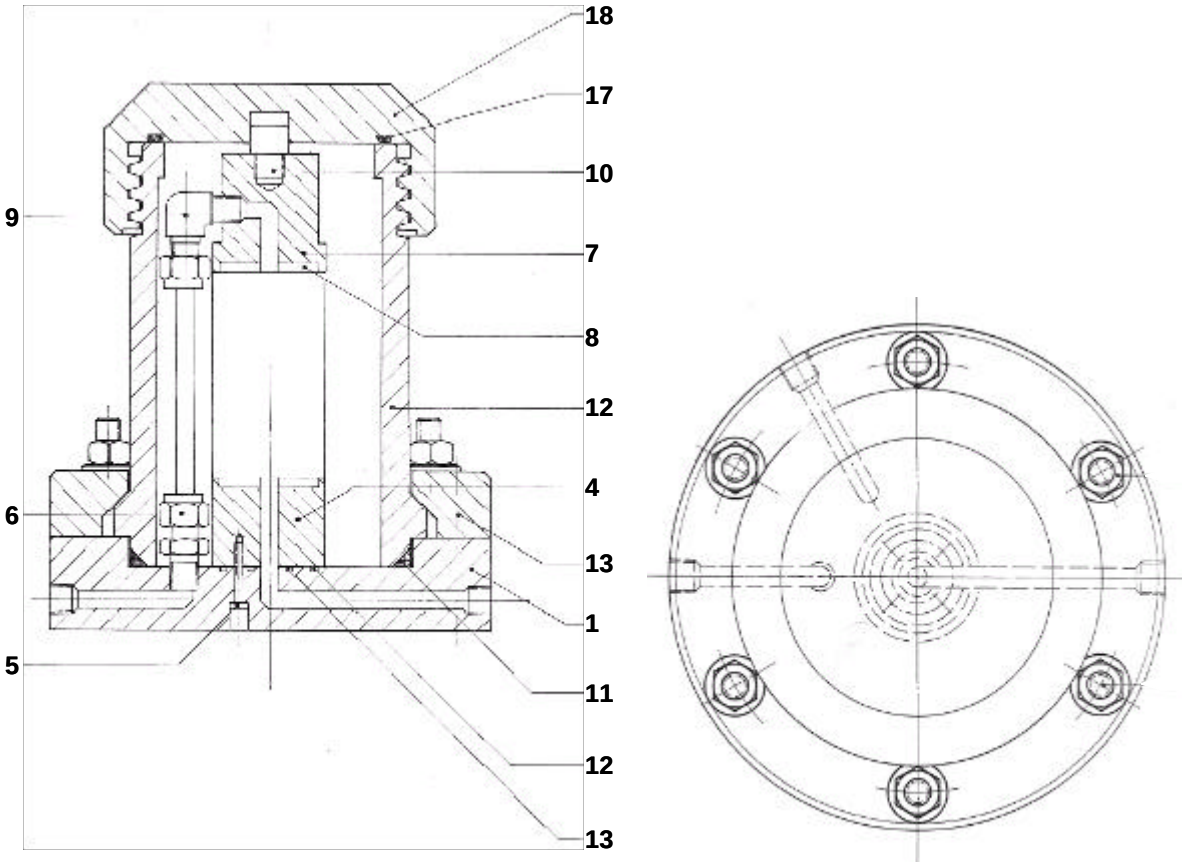

Figure 3: Schematic design of the triaxial cell type 1 used for the gas permeability and breakthrough tests

Figure 4: Triaxial cell type 2

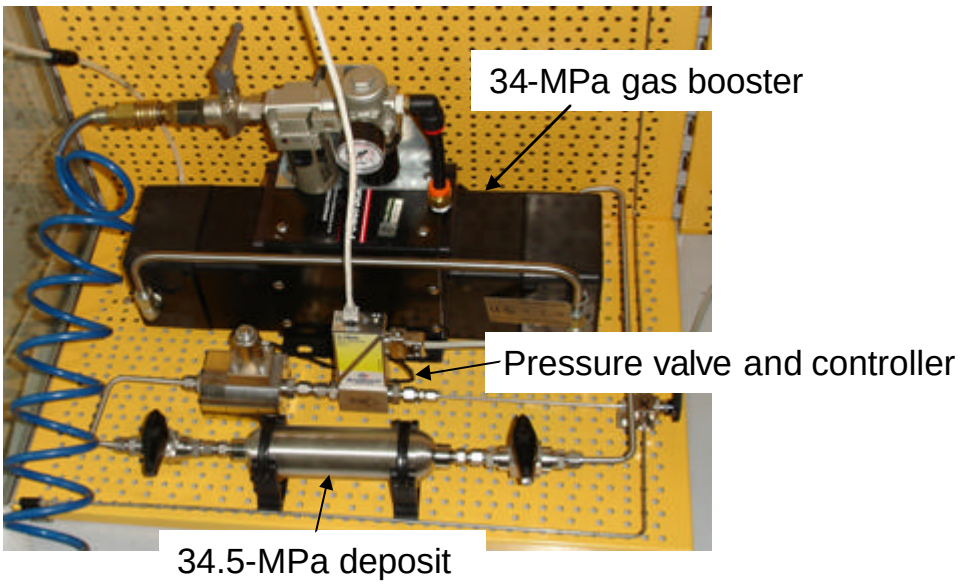

Figure 5: Gas-booster and high-pressure deposit to supply gas to the injection pressure buffer and to the pressure accumulator applying confining pressure in the high-pressure line

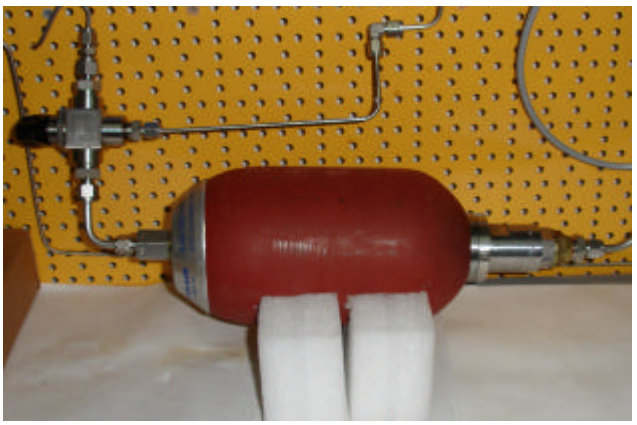

Figure 6: Pressure accumulator to apply high confining pressure

3.2 SAMPLE PREPARATION AND TEST PROCEDURE

The samples were drilled from the BDR-1 core in a sense perpendicular to bedding and the ends were later lathed to assure their parallelism. The resulting specimens were 1.2-3.0 cm in height and 9.2 cm^2 in surface area. They were wrapped in a rubber sleeve that shrank forming a water-resistant seal (Cold Shrink™ Connector Insulator, except sample OPA1) and then in a thick latex membrane with porous stones on top and bottom to sit the set in the triaxial cell pedestal (Figure 7).

Figure 7: Appearance of an Opalinus clay sample drilled for a gas test, wrapped in the shrinking rubber sleeve (black) and in the latex membrane (red)

Once the triaxial cell was filled with water it was pressurised to 8 MPa and a gas injection pressure of 0.5 MPa was applied to the top of the sample. The pressure was increased by 0.5 MPa every 24 h, until reaching a value of 7 MPa. Then the cell was moved to the high-pressure line (except in tests OPA2 and OPA5), in which a confining pressure of 15 MPa was applied, either in steps or suddenly. The injection pressure was also increased up to a value of 14 MPa. Then, in tests OPA1, OPA3 and OPA4, the confining pressure was increased to 19 MPa and the injection pressure to 18 MPa, which was the maximum value allowed by the setup. The pressure paths followed in the test are shown in Figure 8. All pressure values are absolute.

After the gas breakthrough tests, samples OPA3 and OPA4 were saturated with deionised water injected through the bottom surface at a pressure of 0.6 MPa (test with OPA4 still ongoing). The sample was kept in the same triaxial cell, and the confining pressure applied during saturation was 1.5 MPa. After full saturation the water pressure at the bottom was increased to 1.2 MPa and a backpressure of 0.6 MPa was applied on top. For that, a GDS pressure/volume controller was used, what allowed to measure the water outflow and compute the hydraulic conductivity applying Darcy's law (Figure 9).

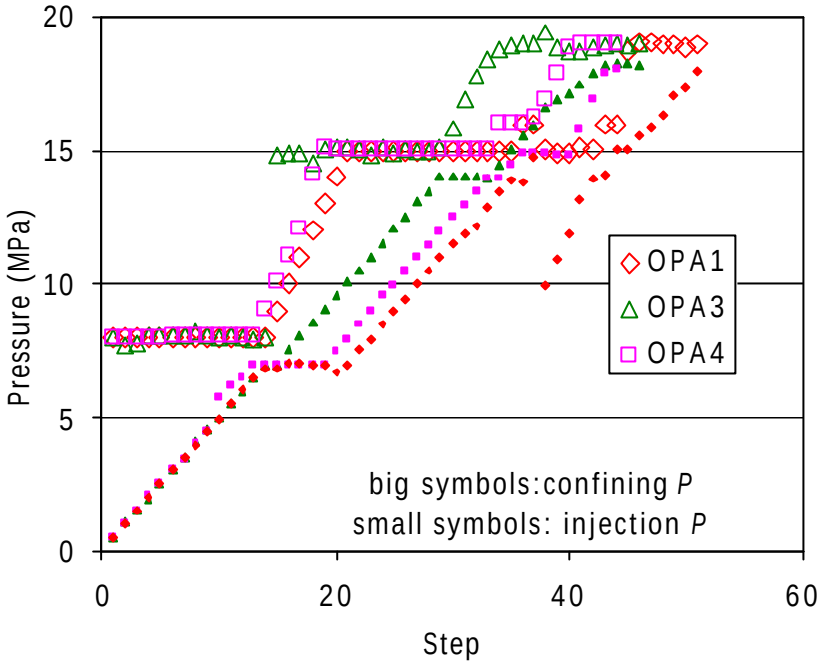

Figure 8: Pressure paths followed in the gas breakthrough tests (tests OPA2 and OPA5 followed only Phase 1 under confining pressure 8 MPa)

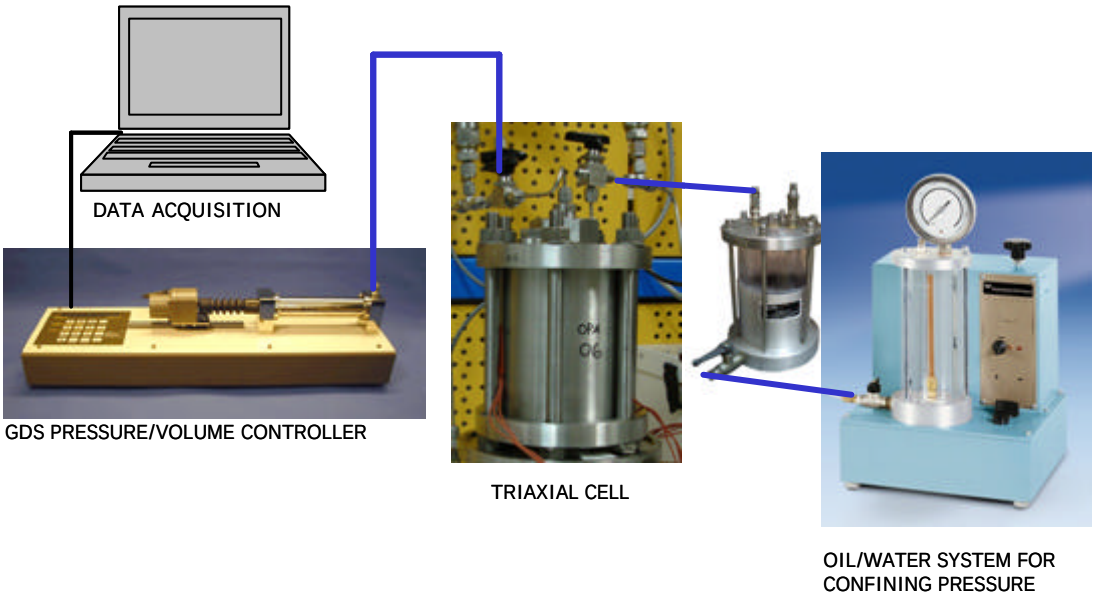

Figure 9: Setup for the water permeability tests

3.3 GAS PERMEABILITY COMPUTATION

The intrinsic permeability of the material could not be directly obtained from the measurements performed, since to determine the intrinsic permeability with air flow the sample must be completely dry. When there are two fluids present in the porous material (gas and water in this case), the permeabilities of each fluid depend upon the saturation of each fluid: these are called effective permeabilities. Hence the value obtained in the determinations is the intrinsic permeability measured with gas flow, k_{ig}, multiplied by the relative permeability to gas, k_{rg}. The relative permeability to gas is the ratio of the effective permeability of gas at a particular saturation to the absolute permeability of gas at total gas saturation, i.e. in completely dry material, where the k_{rg} value would be 1.

To compute the permeability the outflow measurements were used, applying the following equation for incompressible media with compressible pore fluids (Scheidegger 1974):

$$k_{ig} \cdot k_{rg} = \frac{Q_m \times m_g \times L \times 2P_m}{A \times (P_{up}^2 - P_{dw}^2)} \quad [1]$$

where Q_m is the measured flow (volume of fluid as a function of time), A is the sample surface area, μ_g is the fluid dynamic viscosity, L is the sample length and P_{up} and P_{dw} are the upstream and downstream pressures applied at the top (inlet) and the bottom (outlet), respectively, of the sample, and P_m is the pressure of the measured flow (in our case, due to the STP conditions of the gas mass flowmeters, the atmospheric pressure). In turn gas permeability, k_g, can be computed taking into account the gas density and viscosity change with upstream or downstream pressures (P):

$$k_g = \frac{r_g \times g \times P}{m_g} \times k_{ig} \times k_{rg} \quad [2]$$

It is considered that the viscosity of nitrogen did not change during the tests because they were isothermal, whereas density changed with pressure. The change in density was considered as that of an ideal gas, and thus computed as the product of the density of nitrogen at atmospheric pressure times the pressure of the flow used for the computation (*i.e.* atmospheric pressure). This solution assumed that steady state flow was established, what meant that the quantity of gas exiting the sample in the low pressure side was equal to that entering the sample in the high pressure side. In any case, the underestimation of the calculated permeability coefficients should be less than 1.3%.

4 Results

Five gas permeability tests were performed in triaxial cells with Opalinus clay samples obtained by drilling from the BDR-1 core in the sense perpendicular to bedding. Table I summarises the characteristics of the specimens used.

Table I: Characteristics of the specimens used for gas permeability tests

Test reference	Height (cm)	Surface area (cm^2)	Initial ρ_d (g/cm^3)	Initial w (%)	Initial S_r (%)	Final ρ_d (g/cm^3)	Final w (%)	Final S_r (%)
OPA1	3.01	9.05	2.29	4.8	72	2.29	4.8	72
OPA2	2.42	9.24	2.32	2.1	34	2.34	5.6	98
OPA3	2.84	9.19	2.29	5.6	84	2.22	5.7	69
OPA4[a]	1.23	9.29	2.27	4.8	67			
OPA5	1.96	9.11	2.33	5.8	96	2.33	5.8	96
Average	2.29±0.72	9.18±90.10	2.31±0.02	4.6±1.7	71±27	2.29±0.06	5.5±0.5	84±15

[a]test still in course, values not confirmed

Test OPA1

The pressure path and the flow measured during test OPA1 are shown in Figure 10. Once the triaxial cell type 1 was filled with water it was pressurised to 8 MPa and a gas injection pressure of 0.5 MPa was applied to the top of the sample and increased every 24 h (approximately). Every time the injection pressure was increased, what implied a decrease in effective pressure, the flow increased. When the injection pressure reached 7 MPa, the confining pressure was increased stepwise until 15 MPa. During this phase the flow decreased, what could reflect the effect of confining pressure on permeability (Figure 11). The injection pressure was subsequently increased until 14 MPa, resulting in a progressive increase in flow that would be linked to the reduction in effective stress. Finally, the confining pressure was increased to 16 MPa (the maximum allowed in the low-pressure line equipment) and the injection pressure to 15 MPa. This situation was kept for 7 days. Then the cell was moved to the high-pressure line, in which a confining pressure of 15 MPa and an injection pressure of 8 MPa –that was progressively increased to 14 MPa– were applied. Finally, the confining pressure was increased to 19 MPa and the injection pressure to 18 MPa, which was the maximum value allowed by the setup. Again, the flow reflected the changes in the stress conditions, decreasing with the increase in confining pressure and increasing with the reduction in effective pressure caused by the injection pressure rise (Figure 12). Nevertheless, the flows measured in the high-pressure line were lower than those previously measured in the low-pressure line for similar pressures, what could be due to irreversible changes occurred to the sample during the variation in stress conditions caused when changing the cell from the low- to the high-pressure line.

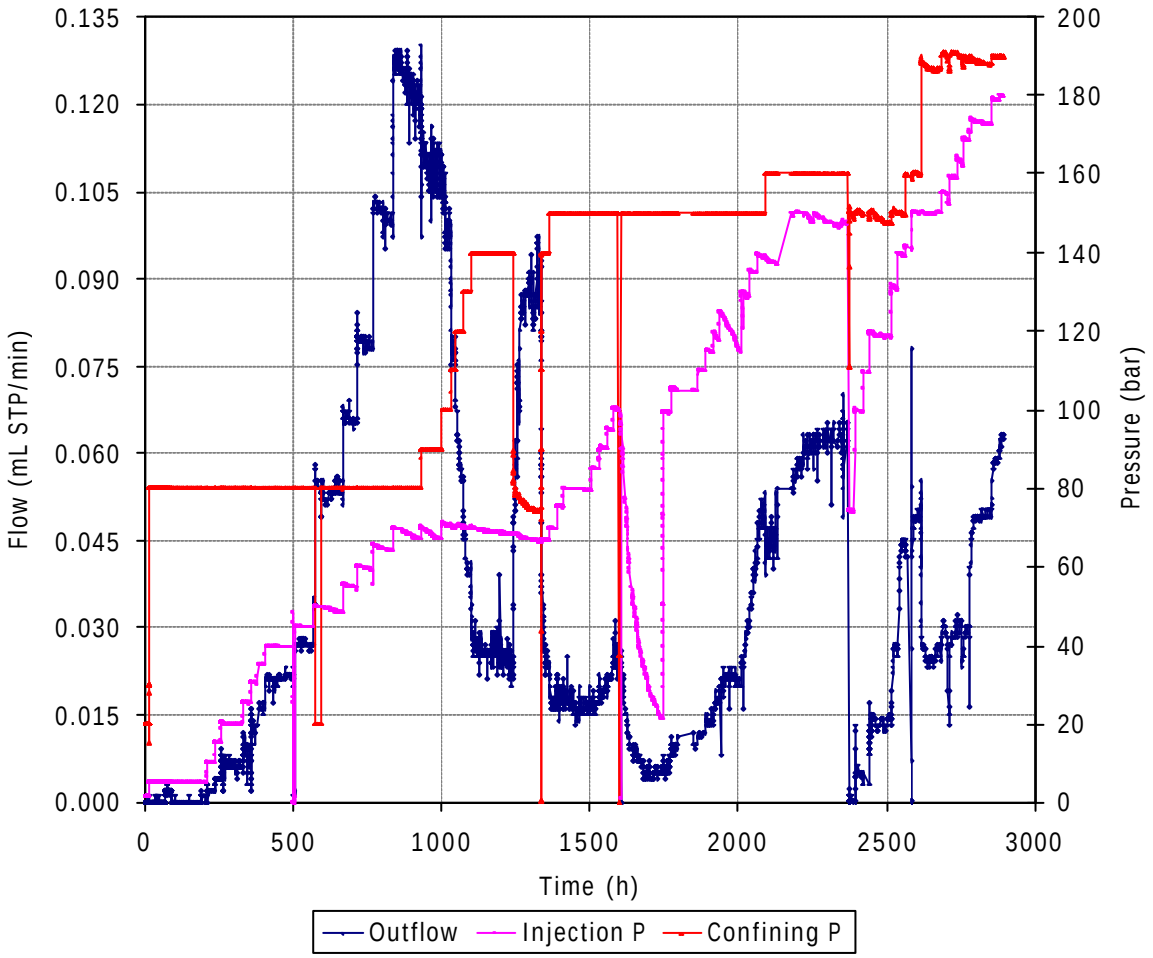

Figure 10: Evolution of injection and confining pressure and outflow in test OPA1

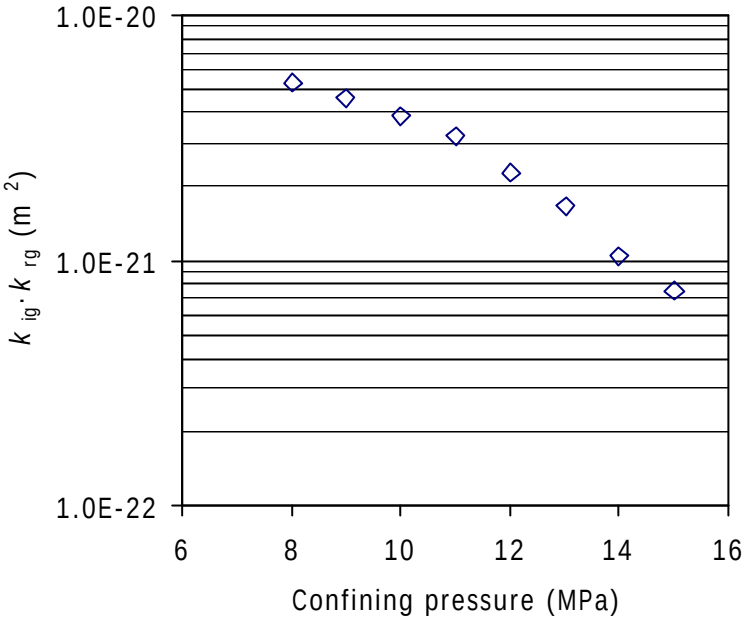

Figure 11: Change of gas permeability with the increase of confining pressure for an injection pressure of 7 MPa and atmospheric backpressure in test OPA1 (tentative values)

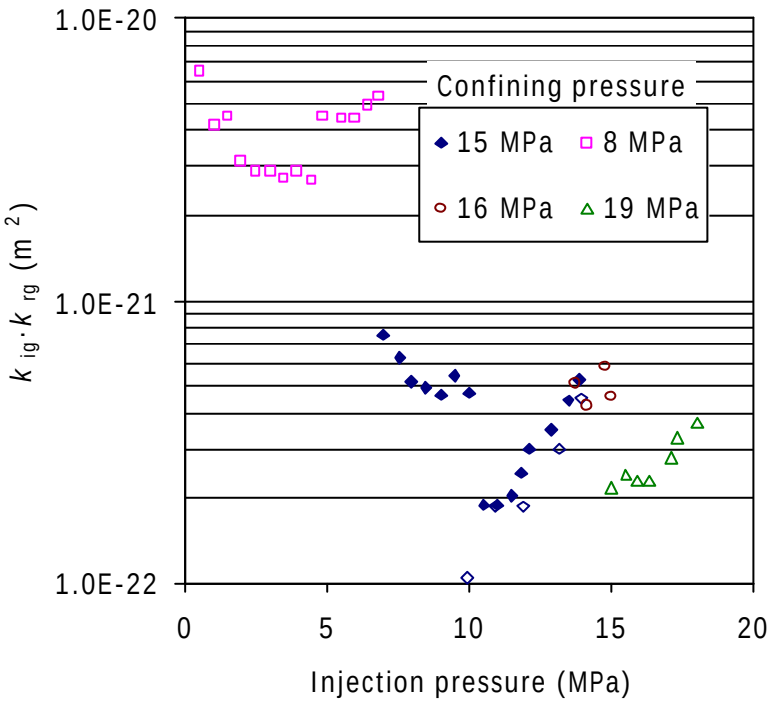

Figure 12: Gas permeability measured for different confining and effective pressures in test OPA1 (tentative values)

Upon dismantling the sample appeared consistent (Figure 13) and no significant features could be observed under the stereomicroscope, except for a carbonate vein on the upper surface that did not have continuity in depth (Figure 14).

Figure 13: Final appearance of sample OPA1

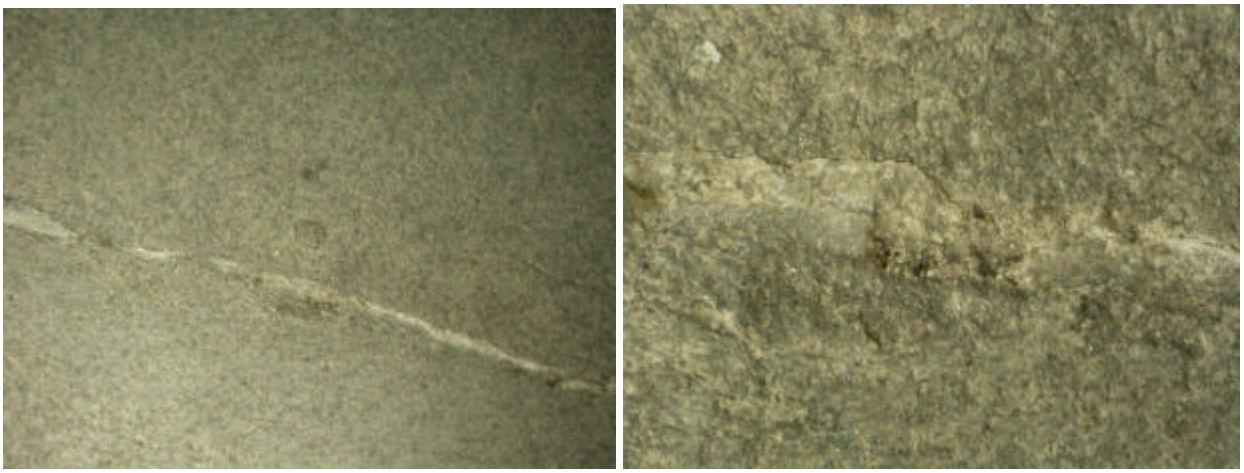

Figure 14: Final appearance of OPA1 under the stereomicroscope

Test OPA2

The pressure path and the flow measured during test OPA2 are shown in Figure 15. The triaxial cell type 2 was filled with water and pressurised to 8 MPa. A gas injection pressure of 0.5 MPa was applied to the top of the sample and increased every 24 h (approximately) by 0.5 MPa until reaching 7 MPa. The flows measured were very low, and they tended to increase as the injection pressure increased, but not enough to result in a permeability increase (Figure 16, in which only the values computed after the breakdown are shown). When the confining pressure was increased to 15 MPa the membrane covering the specimen was perforated and the test had to be suspended. This perforation could be related to a lateral notch initially present in the sample, and as a result of it the sample became completely damaged (Figure 17).

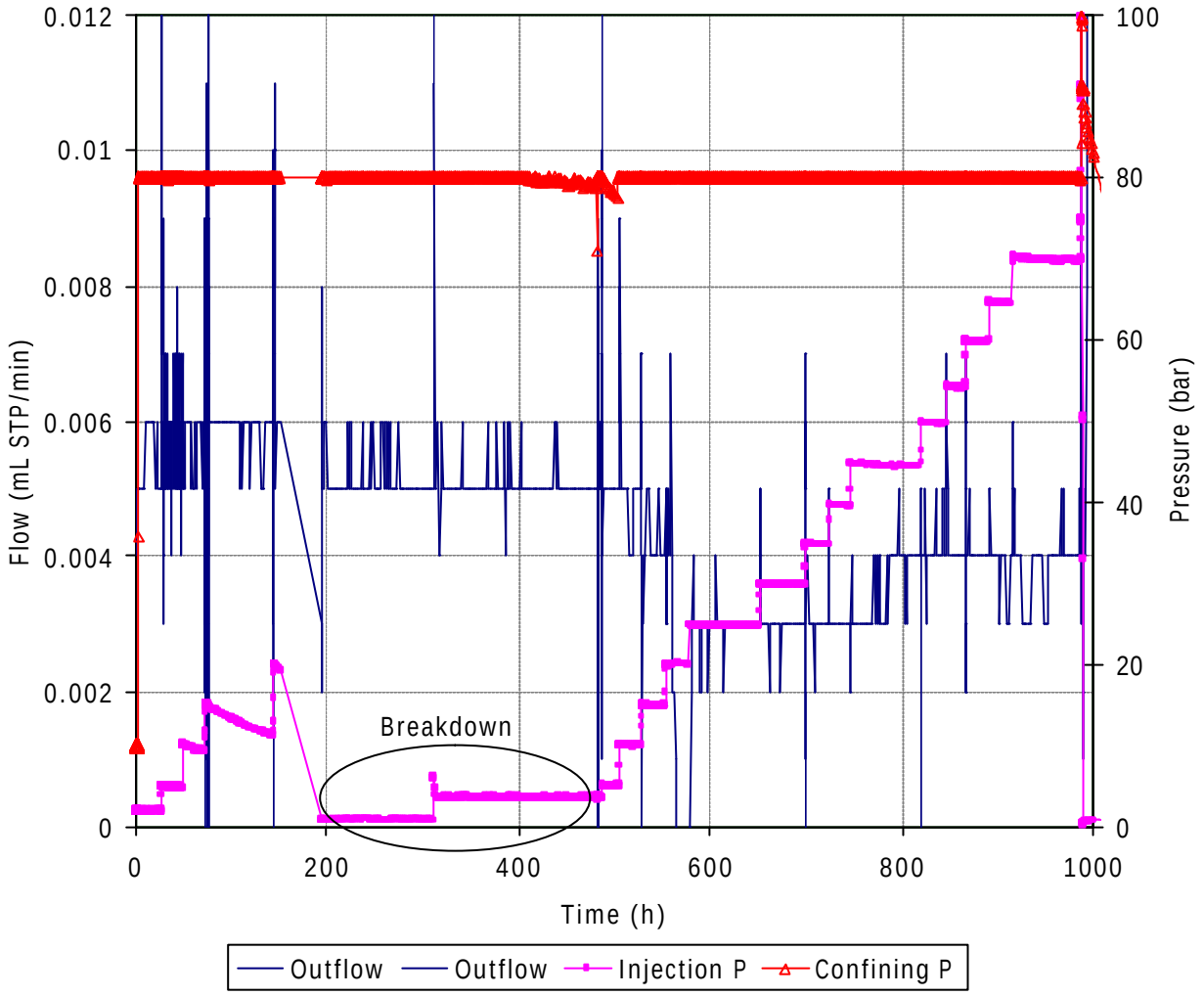

Figure 15: Evolution of injection and confining pressure and outflow in test OPA2

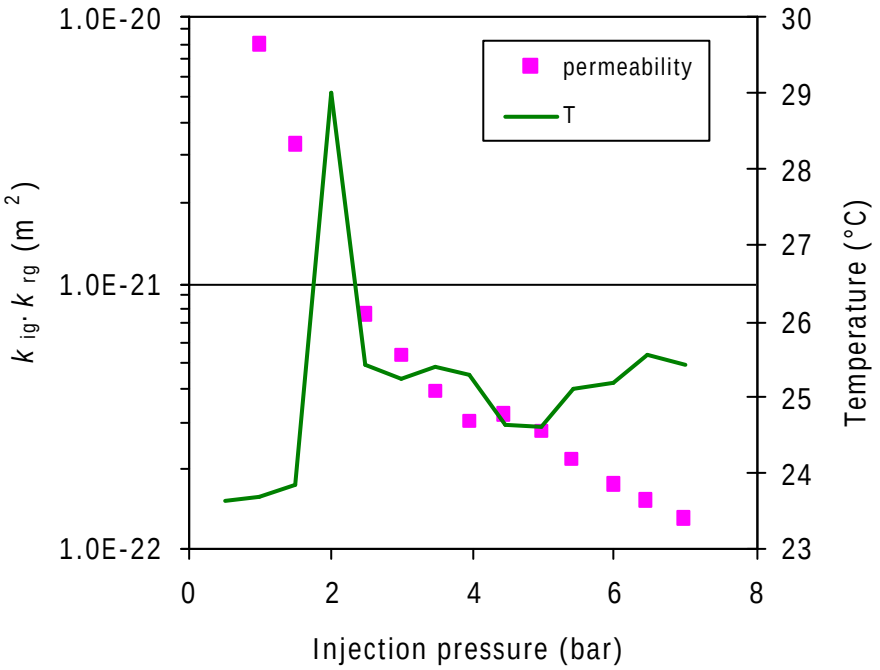

Figure 16: Change of gas permeability with the increase of injection pressure for a confining pressure of 8 MPa and atmospheric backpressure in test OPA2 (tentative values)

Figure 17: Initial and final appearance of sample OPA2

Test OPA3

This sample (Figure 18) was mounted in the triaxial cell type 1 which was initially set in the high-pressure line, for which reason the control of the confining pressure was less steady. The pressure path followed during the test and the flow measured are shown in Figure 19. Initially the cell was pressurised to 8 MPa and a gas injection pressure of 0.5 MPa was applied to the top of the sample and increased every 24 h (approximately). When the injection pressure reached 7 MPa, the confining pressure was increased to 15 MPa. The injection pressure was subsequently increased until 14 MPa, resulting in a progressive increase in flow that would be linked to the reduction in effective stress. Afterwards, the confining pressure was stepwise increased to 19 MPa and the injection pressure to 18 MPa. This last pressure situation was kept for 27 days.

The flows measured during the test (time-integrated value of intermittent flow) were always very low, in most of the cases below the turndown value (accurate detection limit) of the flowmeters, for which reason they can only be used as a qualitative indicator of the actual gas flow and the gas permeability values computed are only tentative (Figure 20). Nevertheless, the flow slightly reflected the changes in the stress conditions, tending to decrease with the increase in confining pressure and to increase with the reduction in effective pressure caused by the injection pressure rise. In spite of some flow spikes in the gas flow measurements, an important decrease of effective stress (to values around 1 MPa) was needed to observe a "steady" gas flow. This fact could be related to the formation of gas pathways that remained later open.

Figure 18: Appearance of specimen OPA3 after drilling from the core

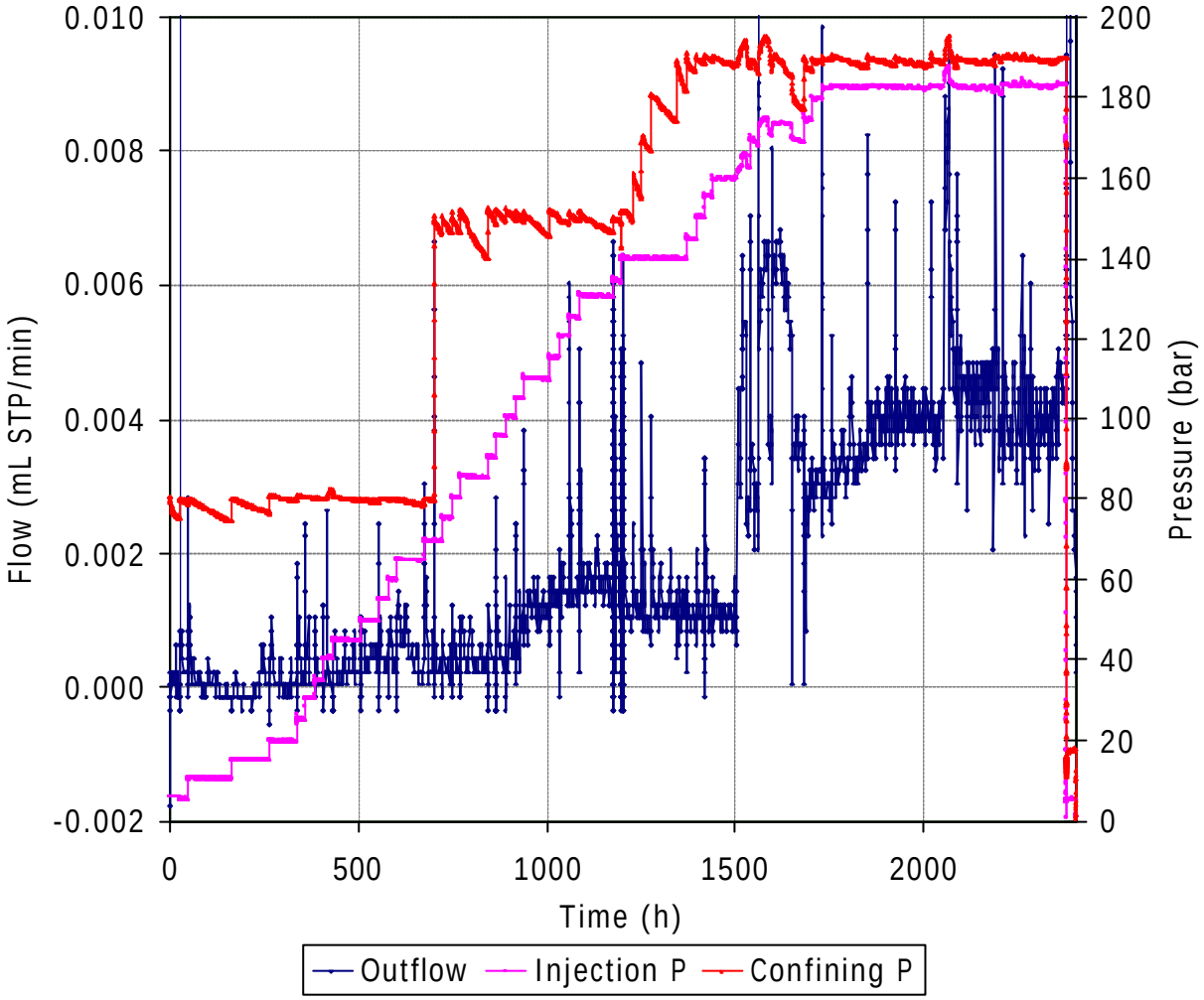

Figure 19: Evolution of injection and confining pressure and outflow in test OPA3

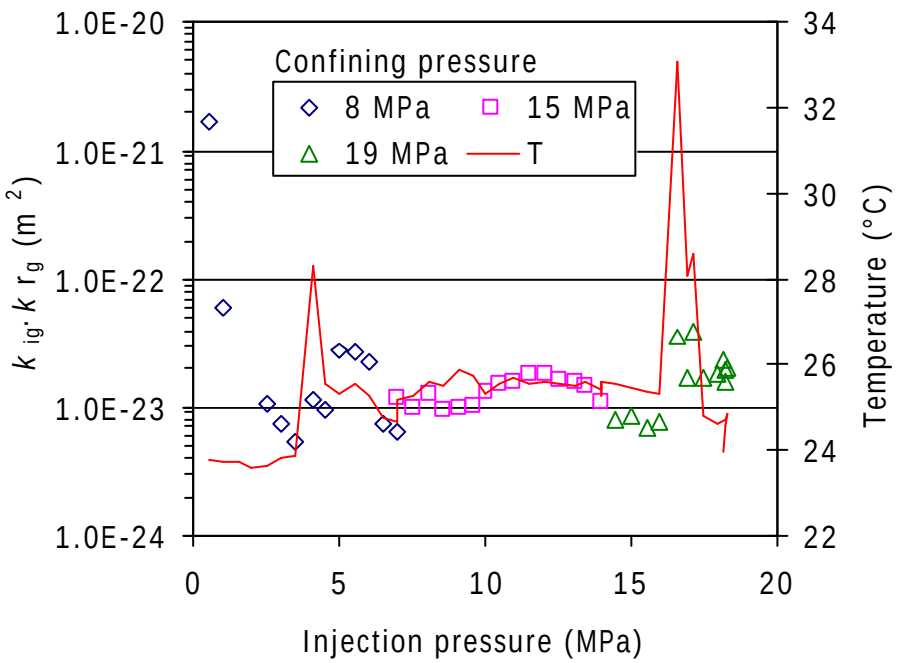

Figure 20: Change of gas permeability with the increase of injection pressure for different confining pressures and atmospheric backpressure in test OPA3 (tentative values)

After the gas permeability test, the cell was moved to a water constant head permeameter (Figure 9) and the sample was saturated with deionised water injected through the bottom surface at a pressure of 0.6 MPa. The sample was kept in the same triaxial cell, and the confining pressure applied during saturation was 1.5 MPa. After full saturation the water pressure at the bottom was increased to 1.2 MPa and a backpressure of 0.6 MPa was applied on top and the water outflow measured. The hydraulic conductivity (k_w) measured in the direction perpendicular to bedding was $2.2 \cdot 10^{-11}$ m/s, corresponding to an intrinsic permeability (k_{iw}) of $2.3 \cdot 10^{-20}$ m^2.

Test OPA4

This sample was mounted in the triaxial cell type 2. The pressure path followed during the test and the flow measured are shown in Figure 21. Initially the cell was pressurised to 8 MPa and a gas injection pressure of 0.5 MPa was applied to the top of the sample and increased every 24 h (approximately). When the injection pressure reached 7 MPa, the confining pressure was increased stepwise to 15 MPa. The injection pressure was subsequently increased also stepwise up to 14 MPa. Afterwards, the confining pressure was increased to 16 MPa and the injection pressure to 15 MPa and these values were kept for 9 days. After changing the cell to the high-pressure line, the confining pressure was increased stepwise up to 19 MPa while the injection pressure was kept at 15 MPa. Afterwards the injection pressure was progressively increased to 18 MPa (the maximum allowed by the setup). This last pressure situation was kept for 47 days.

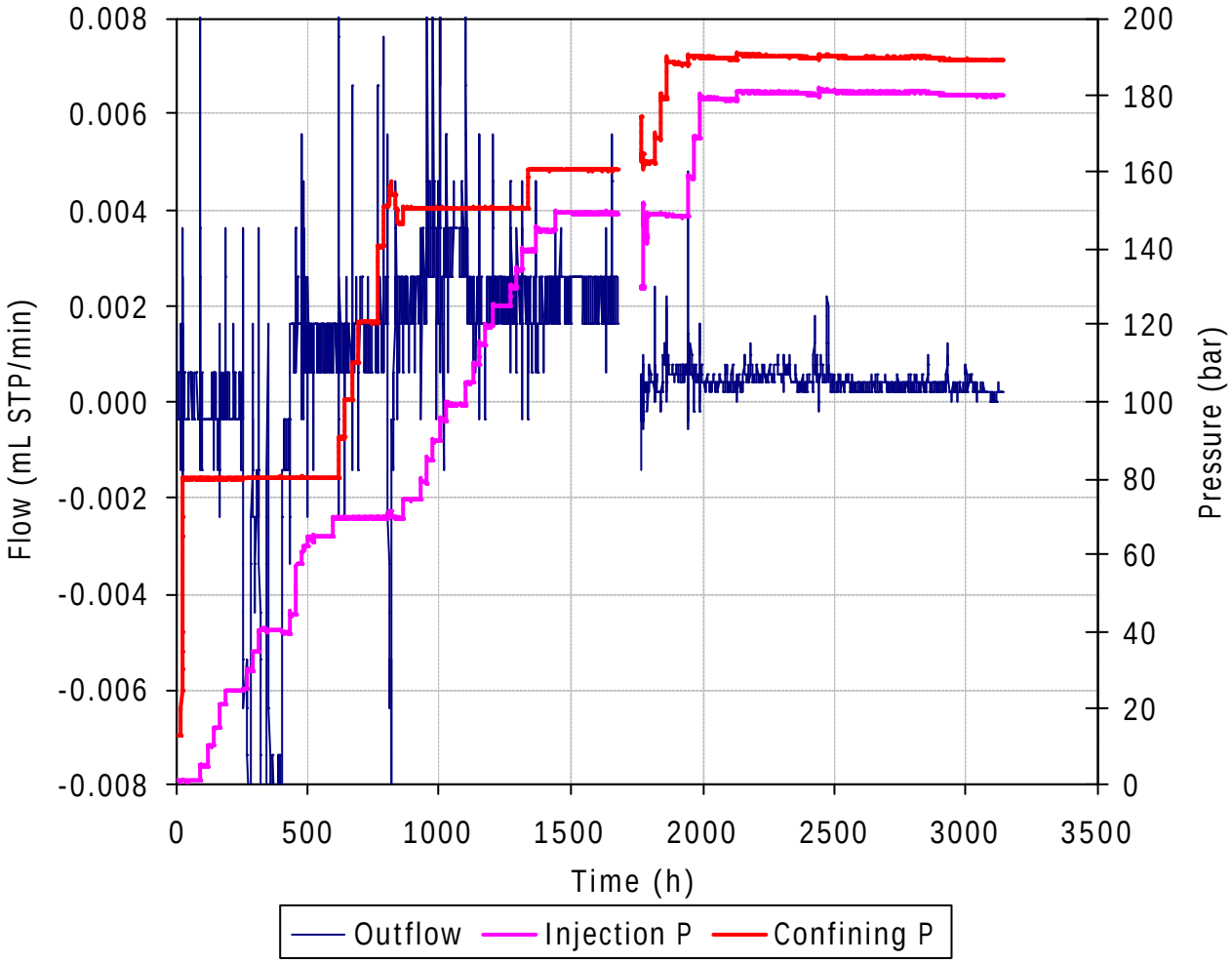

Figure 21: Evolution of injection and confining pressure and outflow in test OPA4

The flows measured were always very low, below the turndown value of the flowmeters, for which reason all the gas permeability values computed are tentative. They show a trend for permeability to decrease as the confining and injection pressures were higher (Figure 22). When moved to the high-pressure line, the flow values showed less noise and an overall lower value, due to the different range of the flowmeters used in the two lines (10 *vs.* 2 cm^3 STP/min). In both cases, gas flow showed spikes.

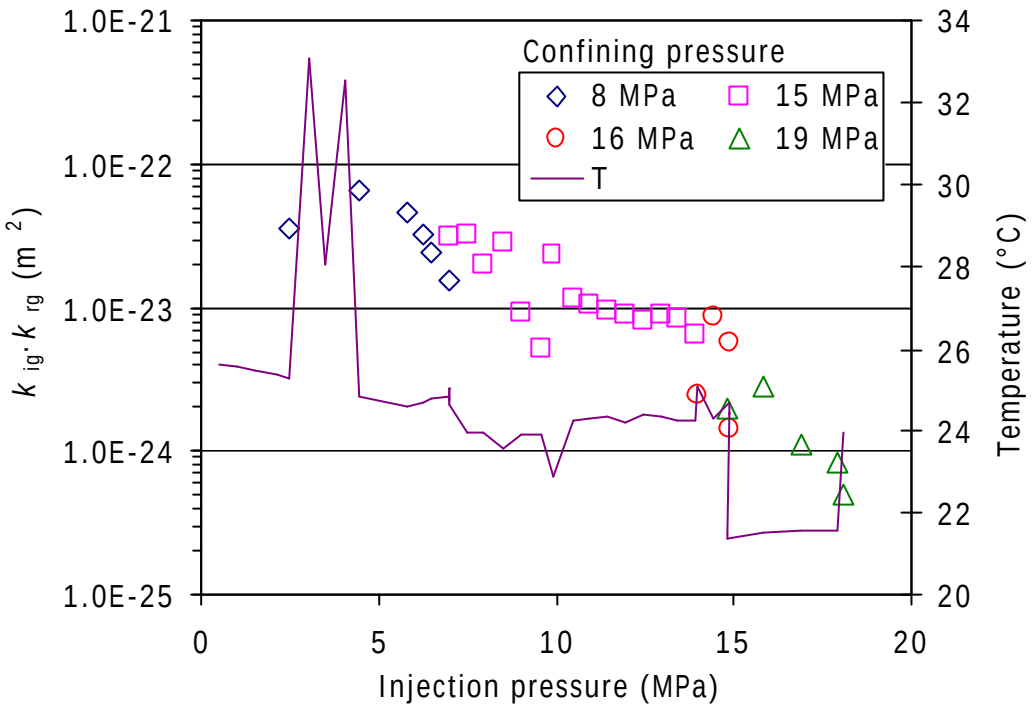

Figure 22: Change of gas permeability with the increase of injection pressure for different confining pressures and atmospheric backpressure in test OPA4 (tentative values)

After the gas permeability test, the cell was moved to a water constant head permeameter (Figure 9) and the sample was saturated with deionised water injected through the bottom surface at a pressure of 0.6 MPa. The sample was kept in the same triaxial cell, and the confining pressure applied during saturation was 1.5 MPa.

Test OPA5

This sample was mounted in the triaxial cell type 2. The pressure path and the flow measured during test OPA5 are shown in Figure 23. The triaxial cell was filled with water and pressurised to 8 MPa. A gas injection pressure of 0.5 MPa was applied to the top of the sample and increased every 24 h (approximately) by 0.5 MPa. The flows measured were very low, an order of magnitude lower than the turndown value of the flowmeter used, hence the permeability values computed are not reliable (Figure 24). When the injection pressure was increased to 6 MPa the membrane covering the specimen was perforated and the test had to be suspended because the sample became completely damaged (Figure 25).

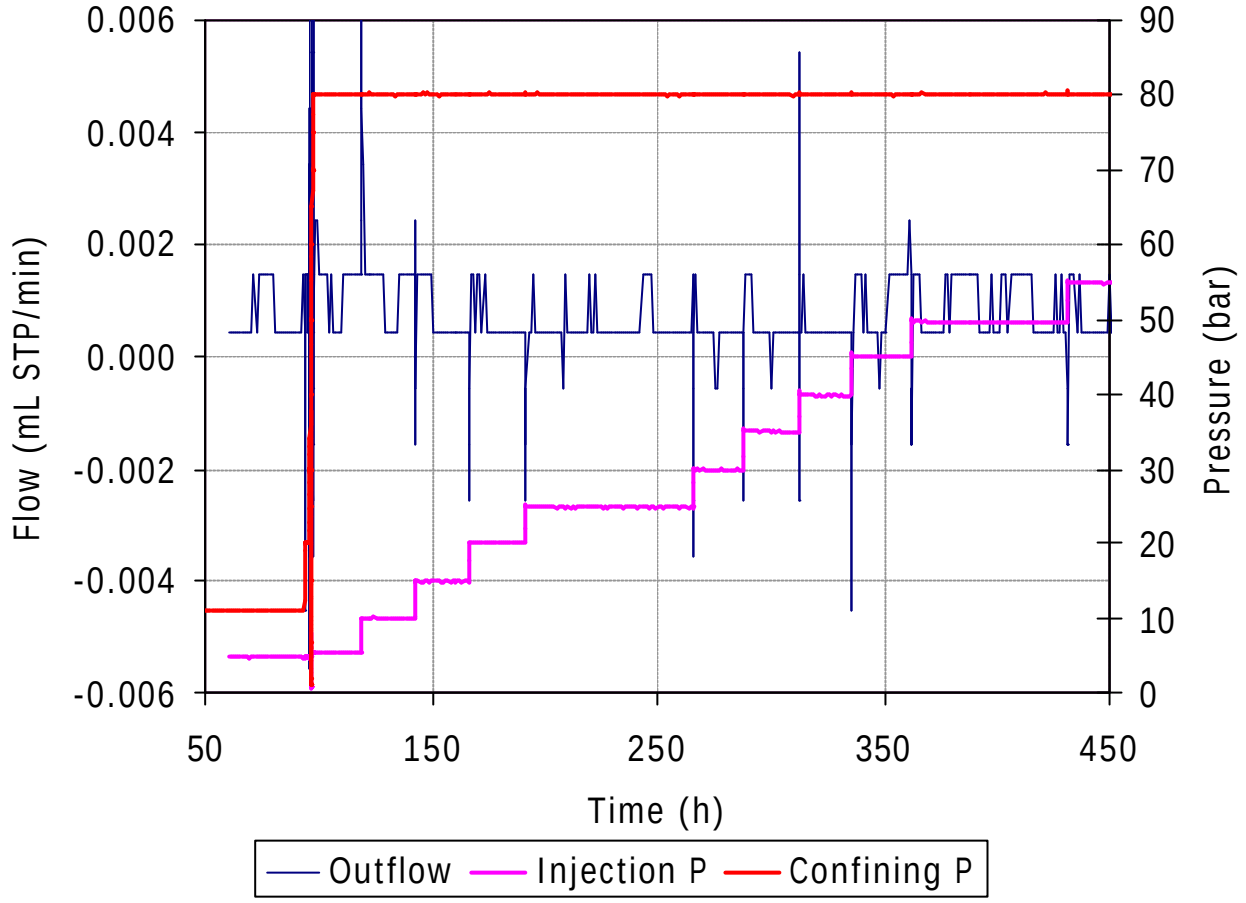

Figure 23: Evolution of injection and confining pressure and outflow in test OPA5

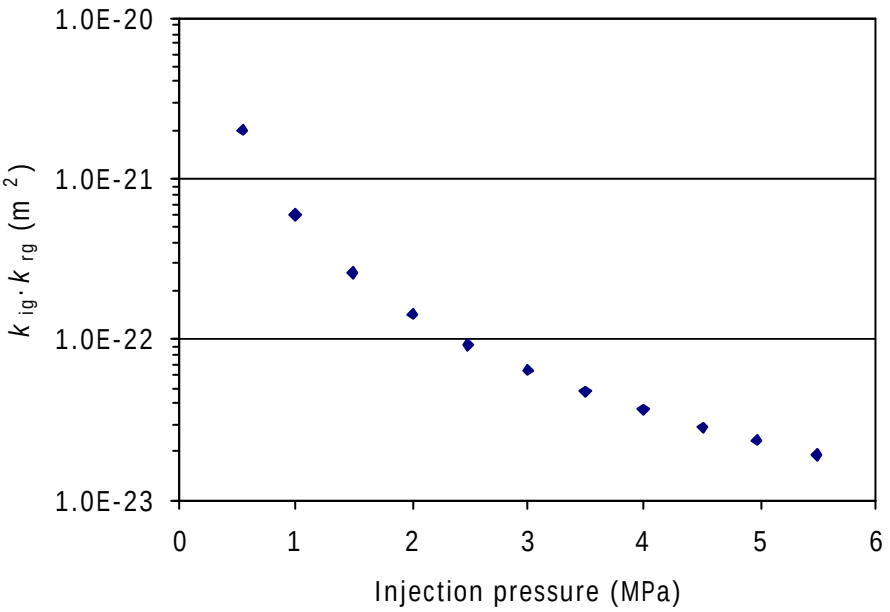

Figure 24: Change of gas permeability with the increase of injection pressure for confining pressure 8 MPa and atmospheric backpressure in test OPA5 (tentative values)

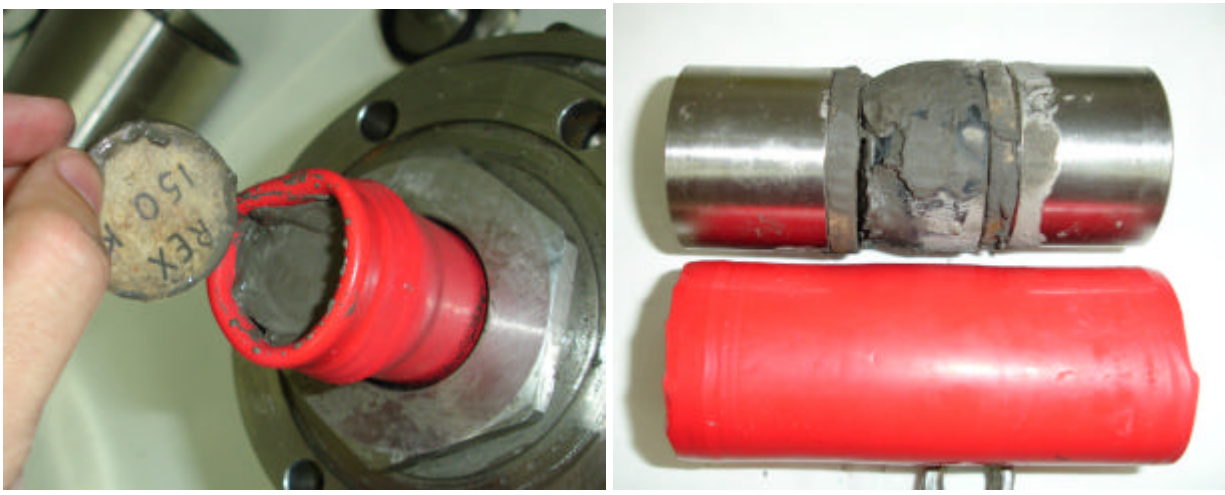

Figure 25: Final appearance of specimen OPA5

Summary of results

Five gas permeability tests were performed in triaxial cells with Opalinus clay samples obtained by drilling from the BDR-1 core in the sense perpendicular to bedding. All of them started with a confining pressure of 8 MPa, which is slightly higher than the maximum *in situ* stress. The injection pressure was slowly increased until a value of 7 MPa. In three of the tests the confining pressure was increased to 15 MPa and the injection pressure to 14 MPa. This pressure situation was prolonged for 7 days in test OPA1 and 9 days in test OPA4. Later, the pressures were increased in some tests up to values of 19 MPa for the confining pressure and 18 MPa for the injection pressure (the maximum allowed by the setup), and kept constant for 27 days in test OPA3 and 47 days in test OPA4.

Except for test OPA1 no correctly measurable outflow was detected during the tests, because the values were below the turndown value (accurate detection limit) of the flowmeters used. In test OPA1 a different thermoretractable tube, which needed heat to retract around the sample, was used to wrap the sample. There is the possibility that this sleeve was not as effective as the other retractable tubes used in the other samples, and some flow could have occurred along the sample periphery, what would explain the higher flows measured.

Overall, with the devices available, it was not possible to properly measure gas permeability and the gas breakthrough pressure for the Opalinus clay with a dry density of 2.29±0.06 g/cm^3 and a water content of 5.5±0.5% (S_r=84±14%) in the sense perpendicular to bedding was higher than 18 MPa.

However, the flowmeters did record values during the tests, a time-integrated value of intermittent flow which was below their turndown value. If this flow were considered representative of the actual flow, gas permeability ($k_{ig} \cdot k_{rg}$, *i.e.* intrinsic gas permeability times relative gas permeability) could be computed and the values shown in Figure 26 would be obtained. The values were in the range from 10^{-20} to 10^{-24} m^2 (average k_g of $1 \cdot 10^{-15}$ m/s) and tended to decrease with the confining and injection pressure increase. Whereas the decrease of permeability with confining pressure is readily understandable, the decrease in permeability with injection pressure was not to be expected beforehand, since the increase in injection pressure under constant confining pressure implied a decrease in effective stress and in fact a flow increase. It must be taken into account that for the computation of permeability the injection pressure is also considered (Equation 1), and its increase implied a decrease in permeability that could not be compensated by the associated flow increase recorded, which was very low.

The minimum gas permeability values that could be calculated for the turndown value of the lowest range flowmeter (0.04 STP cm^3/min) would range from 10^{-19} to 10^{-22} m^2 (from the lowest to the highest injection pressures). This means that all the values shown in the Figure below 10^{-22} m^2 (and some under 10^{-19} m^2) cannot be considered accurate and must only be taken as representative of qualitative behaviour.

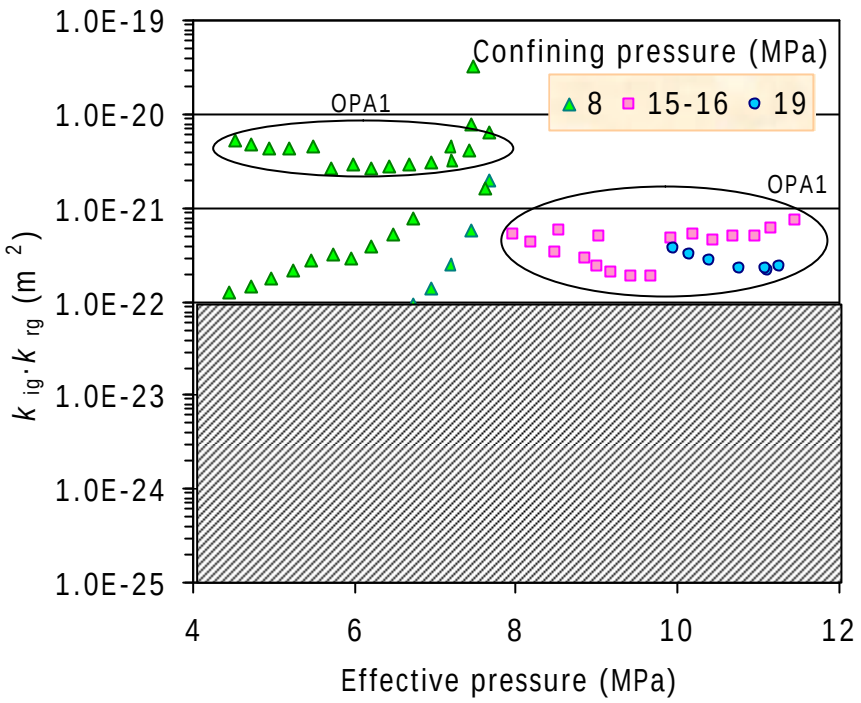

Figure 26: Gas permeability values obtained in samples of Opalinus clay (tentative values, especially those below 10^{-22} m^2; flow along the sample periphery could have taken place in test OPA1)

The hydraulic conductivity (k_w) measured in one of the samples in the direction perpendicular to bedding was $2.2 \cdot 10^{-11}$ m/s, corresponding to an intrinsic permeability (k_{iw}) of $2.3 \cdot 10^{-20}$ m^2. Romero et al. (2012) found for similar void ratios (0.20-0.24) water permeabilities measured in the laboratory an order of magnitude lower. The hydraulic conductivity for the sound shaly facies as determined *in situ* (Marschall et al. 2004) is also lower than the value determined in this work.

Conclusions

The samples used in this research came from borehole BDR-1, drilled in the shaly facies of the Opalinus clay. The gas injection tests reported showed that the breakthrough pressure in the sense perpendicular to bedding was higher than 18 MPa for degrees of saturation of 84±15%. The confining pressures applied in these tests were higher than the maximum *in situ* stress.

The *P* parameter values obtained from water retention curves in a related investigation were between 6 and 34 MPa (Villar & Romero 2012). This parameter is usually related to the air entry value (AEV), which can be calculated from the mercury intrusion porosimetry tests performed in samples from another borehole drilled in the shaly facies and found to be 28 MPa. These values correspond to degrees of saturation of between 80 and 90%, which implies that 2-phase flow (without significant deformation of the pore space) would take place only for

degrees of saturation lower than about 90% (lower if confining is high). For higher degrees of saturation, macroscopic fracture formation (fracing, dependent on the stress state of the material) could be the mechanism for gas flow.

Since it was not possible to determine in the tests presented here the actual breakthrough pressure value, the relationship between the AEV and the breakthrough pressure could not be stated.

References

CORKUM, A.G. AND MARTIN, C.D. 2007. Modelling a mine-by test at the Mont Terri rock laboratory, Switzerland. *Int. J. Rock Mech. Min. Sci*. 44(6): 846-859.

MARSCHALL, P., CROISÉ, J., SCHLICKENRIEDER, L., BOISSON, J.-Y., VOGEL, P., YAMAMOTO, S. 2004. Synthesis of Hydrogeological Investigations at the Mont Terri Site (Phases 1 to 5). Heitzmann, P. ed. 2004: Mont Terri Project- Hydrogeological Synthesis, Osmotic Flow. Reports of the Federal Office for Water and Geology, FOWG, Geology Series No. 6.

ROMERO, E., SENGER, R., MARSCHALL, P.; GÓMEZ, R. 2012. Air tests on low permeability claystone formations. Experimental results and simulations. In: Laloui, L. & Ferrari, A. (Eds.): Multiphysical Testing of Rocks and Shales. Springer Series in Geomechanics and Geoengineering, pp. 69-83. Springer, Berlin.

SCHEIDEGGER, A.E. 1974. *The physics of flow through porous media*. 3rd ed. Toronto : University of Toronto Press, 353 pp.

VILLAR, M.V. AND ROMERO, F.J. 2012. Water retention curves of Opalinus clay. Informes Técnicos CIEMAT 1262. Octubre 2012. CIEMAT, Madrid, 33 pp.